

Accurate Approximation of in-Ecliptic Trajectories for E-Sail with Constant Pitch Angle

Mingying Huo

Department of Aerospace Engineering, Harbin Institute of Technology, Harbin 150001, China

Giovanni Mengali, Alessandro A. Quarta*

Department of Civil and Industrial Engineering, University of Pisa, I-56122 Pisa, Italy

Abstract

Propellantless continuous-thrust propulsion systems, such as electric solar wind sails, may be successfully used for new space missions, especially those requiring high-energy orbit transfers. When the mass-to-thrust ratio is sufficiently large, the spacecraft trajectory is characterized by long flight times with a number of revolutions around the Sun. The corresponding mission analysis, especially when addressed within an optimal context, requires a significant amount of simulation effort. Analytical trajectories are therefore useful aids in a preliminary phase of mission design, even though exact solution are very difficult to obtain. The aim of this paper is to present an accurate, analytical, approximation of the spacecraft trajectory generated by an electric solar wind sail with a constant pitch angle, using the latest mathematical model of the thrust vector. Assuming a heliocentric circular parking orbit and a two-dimensional scenario, the simulation results show that the proposed equations are able to accurately describe the actual spacecraft trajectory for a long time interval when the propulsive acceleration magnitude is sufficiently small.

Keywords: Electric Solar Wind Sail, Trajectory approximation, Mission analysis

Nomenclature

\mathbf{a}	=	propulsive acceleration
a_0	=	parking orbit semimajor axis
a_c	=	spacecraft characteristic acceleration
a_r	=	radial component of propulsive acceleration
a_θ	=	transverse component of propulsive acceleration
\mathcal{A}	=	coefficient, see Eq. (30)
\mathcal{B}	=	coefficient, see Eq. (31)
d	=	dimensionless error in distance
e_0	=	parking orbit eccentricity
F	=	auxiliary function, see Eq. (19)
h	=	osculating orbit specific angular momentum modulus
$\hat{\mathbf{i}}_r$	=	radial unit vector
$\hat{\mathbf{i}}_\theta$	=	transverse unit vector

*Corresponding author

Email addresses: huomingying123@gmail.com (Mingying Huo), g.mengali@ing.unipi.it (Giovanni Mengali), a.quarta@ing.unipi.it (Alessandro A. Quarta)

\hat{i}_x, \hat{i}_y	=	cartesian reference frame unit vectors
O	=	Sun's center-of-mass
r	=	Sun-spacecraft distance (with $r_\oplus \triangleq 1$ au)
t	=	time
u	=	radial component of velocity
v	=	transverse component of velocity
α_n	=	pitch angle
χ	=	auxiliary variable, see Eq. (14)
Δr	=	corrective term in radial distance
θ	=	polar angle
μ_\odot	=	Sun's gravitational parameter
ν	=	true anomaly
ρ	=	dimensionless error in radial distance

Subscripts

0	=	initial, parking orbit
\star	=	limit value
max	=	maximum
num	=	numerical value

Superscripts

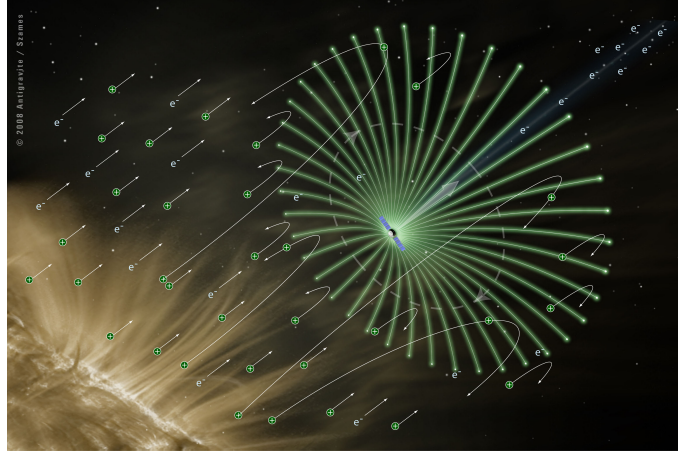
\cdot	=	time derivative
$'$	=	derivative with respect to χ

1. Introduction

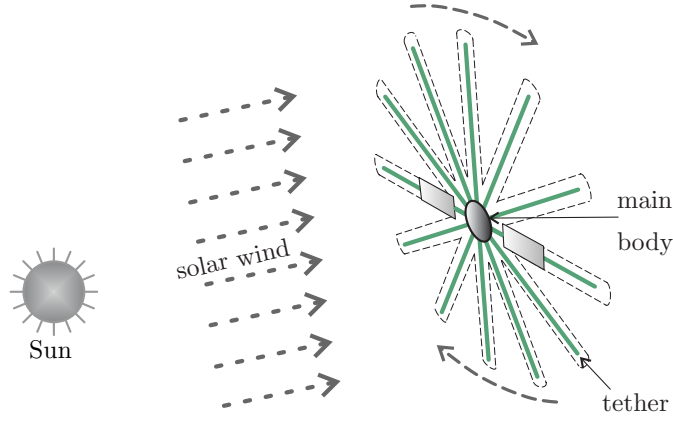
Analytical solutions to continuous-thrust spacecraft dynamics represent a major aid during the preliminary phase of mission design and optimization [1], as they allow a large number of possible choices to be analyzed with a reduced computational effort [2]. In general, such solutions are difficult to obtain and, indeed, are available in a few cases only [3, 4, 5]. Nevertheless, due to their practical implications, a viable and interesting alternative is to resort to a shape-based approach in which the trajectory shape is parameterized with a given analytical function [6, 7, 8], or to approximate the exact solution by solving a simplified set of equations of motion [9, 10, 11].

Within the latter context, [12] have obtained an analytical approximate expression for the heliocentric trajectory of a spacecraft propelled by an Electric Solar Wind Sail (E-sail), see Fig. 1(a), when its propulsive acceleration magnitude is sufficiently small. The E-sail is an innovative concept for spacecraft propulsion, originally proposed by [13]. It uses the solar wind dynamic pressure for producing thrust by exploiting the interaction of solar wind ions with an artificial electric field generated by a number of long and thin charged tethers, which are centrifugally stretched, see Fig. 1(b). The study of this propulsion system has attracted a great interest in the last years. In particular, much efforts have been devoted to the development of mathematical models able to accurately estimate the E-sail propulsive acceleration, yet sufficiently simple to be used for a preliminary mission analysis. In previous works [13, 14, 12], the effect of the E-sail attitude on the thrust modulus and direction was neglected. More precisely, the thrust modulus was assumed to be unaffected by a change in the sail orientation with respect to an orbital reference frame, and the thrust angle has been approximated as equal to one-half of the pitch angle.

The above assumptions, however, are not accurate enough to describe the E-sail thrust vector for mission analysis purposes. For this reason, [15] have proposed a more accurate model of the E-sail thrust, in the form of a polynomial fitting of numerical and experimental data, which takes into account that both thrust modulus and direction depend on the pitch angle. More recently, assuming all of the charged tethers to



(a) Artistic impression. Courtesy of Alexandre Szames, Antigravite (Paris).



(b) Propulsion system conceptual scheme.

Figure 1: Electric solar wind sail concept.

belong to the same nominal plane, [16] have described the E-sail thrust vector with an elegant analytic expression and showed its consistency with the numerical model by [15].

The aim of this paper is to reassess the dynamics of an E-sail-based spacecraft with a low-propulsive acceleration magnitude (i.e. a spacecraft with a high value of mass-to-thrust ratio) using the most recent thrust model, and to improve the accuracy of trajectory approximation using a new, corrective, term. The expressions are given in an analytic form and are obtained assuming the E-sail to maintain a constant pitch angle, that is, a constant attitude with respect to a classical orbital frame. The approach described in the paper is inspired by similar methods developed in the classical literature [11], and the obtained results are both of academic and practical importance.

The paper is organized as follows. The next section introduces the two-dimensional, approximate, trajectory of an E-sail with a fixed attitude and a low propulsive acceleration magnitude, obtained in a parametric form as a function of the spacecraft polar angle. The solution makes use of the latest thrust mathematical model. The soundness and accuracy of the results are checked by simulation, where a numerical integration of the equations of motion is used for comparative purposes. In section 3, a corrective term is introduced to improve the accuracy of the trajectory approximation, and the obtained relationships are compared with the available results from literature. Finally, the last section contains some concluding remarks.

2. Mathematical Model

An E-sail-based spacecraft is initially parked in a heliocentric (Keplerian) elliptic orbit of semimajor axis a_0 and eccentricity $e_0 < 1$. Assuming a two-dimensional mission scenario, introduce a heliocentric polar reference frame $\mathcal{T}(O; r, \theta)$, where r is the Sun-spacecraft distance (with $r_\oplus \triangleq 1$ au), and θ is the polar angle measured counterclockwise from the apse line of the parking orbit, see Fig. 2. Let $\hat{\mathbf{i}}_r$ (or $\hat{\mathbf{i}}_\theta$) be the radial (or transverse) unit vector of the polar reference frame \mathcal{T} .

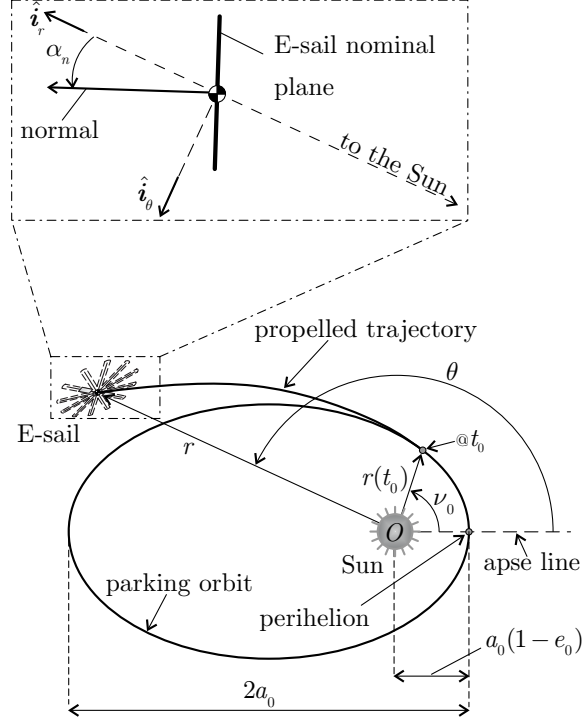


Figure 2: Reference frame and sail pitch angle.

The E-sail propulsive acceleration vector \mathbf{a} depends on the Sun-spacecraft distance r and the E-sail attitude through the pitch angle $\alpha_n \in [-\pi/2, \pi/2]$ rad, defined as the angle between the Sun-spacecraft line and the normal to the E-sail nominal plane in the direction opposite to the Sun [14, 15, 17, 18], see Fig. 2. In this two-dimensional scenario, the pitch angle is the only control variable. Starting from the geometrical analysis by [16], the propulsive acceleration vector \mathbf{a} may be written in a compact form as

$$\mathbf{a} = a_r \hat{\mathbf{i}}_r + a_\theta \hat{\mathbf{i}}_\theta \quad (1)$$

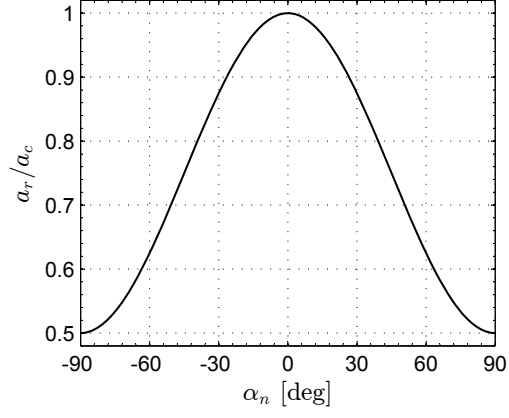
with

$$a_r = \frac{a_c r_\oplus (\cos^2 \alpha_n + 1)}{2r} \quad (2)$$

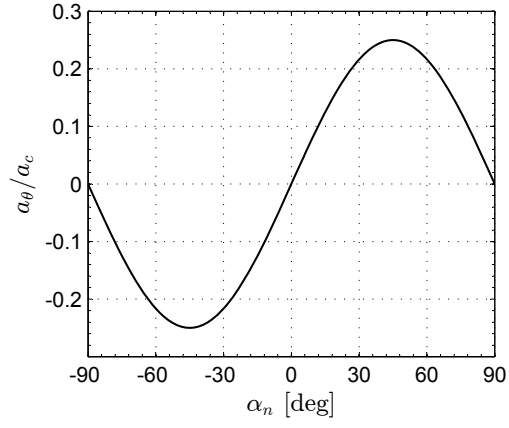
$$a_\theta = \frac{a_c r_\oplus \sin \alpha_n \cos \alpha_n}{2r} \quad (3)$$

where a_c is the characteristic acceleration, that is, the maximum value of $\|\mathbf{a}\|$ when $r = r_\oplus$. Note that in a real case, when the propulsive performance is calculated taking into account the actual tether arrangement, the value of a_c actually depends on both the tether shape and the spacecraft spin rate [19].

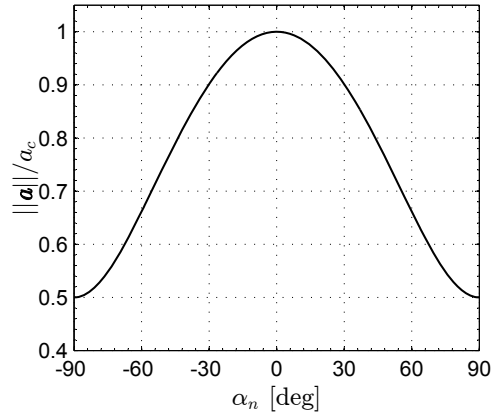
The E-sail propulsive acceleration components are reported in dimensionless form in Fig. 3, as a function of the pitch angle α_n , when $r = r_\oplus$. Recall that the characteristic acceleration coincides with the modulus



(a) Radial component.



(b) Transverse component.



(c) Magnitude.

Figure 3: E-sail (dimensionless) propulsive acceleration as a function of the pitch angle when $r = r_\oplus$.

of the propulsive acceleration of a Sun-facing E-sail (i.e. an E-sail with a pitch angle $\alpha_n = 0$) when the Sun-spacecraft distance is 1 au, see Fig. 3(c). In particular, a_c is a classical performance parameter in the preliminary mission design, as it depends on the spacecraft mass and the E-sail design characteristics such as, for example, the total tether length and the cable electric voltage [20].

Assume the propulsion system to be switched-on at $t_0 \triangleq 0$ and to be working for $t \geq t_0$. Taking into account Eqs. (1)-(3), the E-sail equations of motion in the polar reference frame \mathcal{T} are

$$\dot{r} = u \quad (4)$$

$$\dot{\theta} = \frac{h}{r^2} \quad (5)$$

$$\dot{u} = -\frac{\mu_\odot}{r^2} + \frac{h^2}{r^3} + \frac{a_c r_\oplus (\cos^2 \alpha_n + 1)}{2r} \quad (6)$$

$$\dot{h} = \frac{a_c r_\oplus \sin \alpha_n \cos \alpha_n}{2} \quad (7)$$

where μ_\odot is the Sun's gravitational parameter, u is the radial component of the spacecraft velocity, and h is the modulus of the osculating orbit (specific) angular momentum. Note that the transverse component of the spacecraft velocity v may be written as a function of h and r as

$$v = \frac{h}{r} \quad (8)$$

The differential system of Eqs. (4)-(7) is completed by four initial conditions at time $t = t_0$, viz.

$$r(t_0) = \frac{a_0 (1 - e_0^2)}{1 + e_0 \cos \nu_0} \quad , \quad \theta(t_0) = \nu_0 \quad ,$$

$$u(t_0) = e_0 \sin \nu_0 \sqrt{\frac{\mu_\odot}{a_0 (1 - e_0^2)}} \quad , \quad h(t_0) = \sqrt{\mu_\odot a_0 (1 - e_0^2)} \quad (9)$$

where ν_0 is the spacecraft true anomaly along the (heliocentric) parking orbit when the propulsion system is switched-on, see Fig. 2.

In the special case of a Sun-facing E-sail (i.e., when $\alpha_n = 0$), the fact that h is a constant of motion (see Eq. (7)) allows some noteworthy trajectory characteristics to be found analytically, such as the condition under which a bounded motion can take place [21, 22]. In general, however, for a given time variation of the control variable $\alpha_n = \alpha_n(t)$, the actual E-sail trajectory (that is, the function $r = r(\theta)$ in the polare reference frame) may be obtained in a numerical form only, by solving the corresponding Cauchy problem given by Eqs. (4)-(9). A situation of practical interest occurs when the pitch angle α_n remains constant during the whole spacecraft motion, which amounts to stating that the thrust vector direction in the polar reference frame \mathcal{T} is fixed. This property simplifies the design of the spacecraft thermal control system, as well as that of the power subsystem.

In this context, [23] have recently analyzed the E-sail-spacecraft dynamics using the asymptotic expansion algorithm introduced by [24]. The approximate method proposed by [23], which has also been applied to a solar sail-based mission scenario [25], is able to refine the analytical results obtained by [12] using a different (and more simple) approach. However, the method used by [23] requires a complex analytical analysis of the spacecraft dynamics, which must be written in terms of non-singular orbital elements [24]. Notably, the polar form of the spacecraft trajectory may be accurately described in analytic form without resorting to an asymptotic expansion procedure. This is possible with a suitable refinement of the approach developed in [12], as will be now discussed.

2.1. Mathematical Preliminaries

The first step necessary to get the spacecraft trajectory in a polar form $r = r(\theta)$ is to adapt the accurate thrust model by [16] to suit the procedure developed by [12]. To that end, assume the E-sail pitch angle α_n

to be constant for $t \geq t_0$. From Eq. (7), the magnitude h of the angular momentum increases linearly with time, viz.

$$h(t) = h_0 + \left(\frac{a_c r_\oplus \sin \alpha_n \cos \alpha_n}{2} \right) t \quad (10)$$

where $h_0 \triangleq \sqrt{\mu_\odot a_0 (1 - e_0^2)}$, and subscript 0 denotes a quantity calculated along the parking (heliocentric) orbit. As long as the E-sail attitude is maintained constant with respect to an orbital reference frame, Eq. (10) is exact and provides a first integral of the motion. It may also be substituted into Eq. (6) to facilitate the heliocentric trajectory analysis. However, even with the aid of Eq. (10), a closed-form (exact) solution for the radial component of the spacecraft velocity u cannot be recovered without introducing additional suitable assumptions.

For example, an approximate analytical expression for the spacecraft trajectory can be found when the parking orbit is circular (that is, $e_0 = 0$ and $r(t_0) \equiv a_0$), and the spacecraft characteristic acceleration a_c is sufficiently small compared to the initial gravitational acceleration, or $a_c \ll \mu_\odot/a_0^2$. In particular, neglecting the Earth's orbital eccentricity and assuming $a_0 = r_\oplus = 1$ au, this situation happens when an E-sail-based spacecraft with an high mass-to-thrust ratio leaves the planet's sphere of influence with zero hyperbolic excess velocity. In that case the initial true anomaly can also be assumed to be zero without loss of generality, and the initial conditions become

$$r(t_0) = a_0 \quad , \quad \theta(t_0) = 0 \quad , \quad u(t_0) = 0 \quad , \quad h(t_0) = h_0 = \sqrt{\mu_\odot a_0} \quad (11)$$

while the transverse component of the spacecraft velocity is $v_0 = \sqrt{\mu_\odot/a_0}$.

Since the radial component of the propulsive acceleration (a_r) of a low-performance thruster is much smaller than the local gravitational acceleration (μ_\odot/r^2), and recalling that the parking orbit is circular, the approximation $\dot{u} \approx 0$ may be introduced into Eq. (6) to simplify the analysis of the spacecraft dynamics [12]. The soundness of such an approximation will be justified a posteriori, by comparing the approximate analytical form of the spacecraft trajectory with the numerical results from an orbital simulator. When the condition $\dot{u} = 0$ is substituted into Eq. (6), the Sun-spacecraft distance r may be written as a function of h as

$$r = \frac{\mu_\odot}{a_c r_\oplus (\cos^2 \alpha_n + 1)} \left[1 - \sqrt{1 - \frac{2 a_c r_\oplus (\cos^2 \alpha_n + 1) h^2}{\mu_\odot^2}} \right] \quad (12)$$

where h is an explicit function of time via Eq. (10). Note that, if $\alpha_n > 0$, the term under the square root in Eq. (12) becomes negative when $t > t^*$, where

$$t^* = \frac{2 \mu_\odot / \sqrt{2 a_c r_\oplus (\cos^2 \alpha_n + 1)} - 2 h_0}{a_c r_\oplus \sin \alpha_n \cos \alpha_n} \quad (13)$$

Therefore, Eq. (13) gives an upper bound to the time interval within which the approximation given by Eq. (12) is sound. Figure 4 reports a graphical representation of t^* as a function of α_n and a_c , when $a_0 = r_\oplus$. Assuming $a_c < 0.4 \text{ mm/s}^2$ (low-performance thruster), the term under the square root in Eq. (12) is positive for a long time interval, since the minimum value of t^* is well beyond 10 years. When $\alpha_n = \{-\pi/2, 0, \pi/2\}$ rad (purely radial thrust) Eq. (13) states that $t^* \rightarrow \infty$, in agreement with previous literature [21, 22].

The polar form of the spacecraft trajectory is obtained with the change of variable [12]

$$\chi \triangleq 1 - \frac{2 a_c r_\oplus (\cos^2 \alpha_n + 1) h^2}{\mu_\odot^2} \quad (14)$$

so that Eq. (12) can be rewritten as

$$r(\chi) = \frac{\mu_\odot}{a_c r_\oplus (\cos^2 \alpha_n + 1)} (1 - \sqrt{\chi}) \quad (15)$$

When $\alpha_n = \{-\pi/2, 0, \pi/2\}$ rad, h and χ are both constants of motion, see Eqs. (7) and (14). If, instead, $\alpha_n \neq \{-\pi/2, 0, \pi/2\}$ rad, which implies $\dot{\chi} \neq 0$, Eq. (5) can be turned into a differential equation with

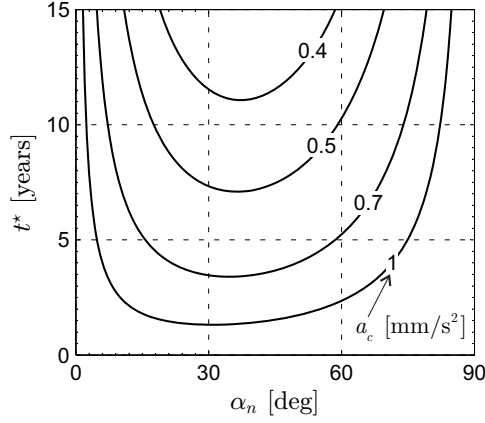


Figure 4: Time t^* as a function of α_n and a_c when $a_0 = r_\oplus = 1$ au, see Eq. (13).

separable variables, viz.

$$\theta' = \frac{\dot{\theta}}{\dot{\chi}} \equiv -\frac{\cos^2 \alpha_n + 1}{2 \sin \alpha_n \cos \alpha_n (1 - \sqrt{\chi})^2} \quad \text{with } \alpha_n \neq \{-\pi/2, 0, \pi/2\} \text{ rad} \quad (16)$$

where the prime symbol denotes a differentiation with respect to the auxiliary variable χ , and $\dot{\chi} = \dot{h}/h'$. Equation (16) can be integrated to yield the polar angle θ as a function of the auxiliary variable χ . The result is

$$\theta(\chi) = \frac{\cos^2 \alpha_n + 1}{2 \sin \alpha_n \cos \alpha_n} [F(\chi_0) - F(\chi)] \quad \text{with } \alpha_n \neq \{-\pi/2, 0, \pi/2\} \text{ rad} \quad (17)$$

where χ_0 is the initial value of χ given by

$$\chi_0 = 1 - \frac{2 a_c a_0 r_\oplus (\cos^2 \alpha_n + 1)}{\mu_\odot} \quad (18)$$

and $F = F(y)$ is an auxiliary function defined as

$$F(y) \triangleq \frac{2}{1 - \sqrt{y}} + 2 \ln(1 - \sqrt{y}) \quad (19)$$

The parametric equation of the (polar) propelled trajectory is given by Eqs. (15) and (17). These equations update the results of [12] with the latest E-sail thrust model introduced by [16]. The approximate time variation of the polar angle may also be analytically obtained by combining Eqs. (17)-(19) with Eqs. (10) and (14).

With the aid of Eq. (15), the radial component of the spacecraft velocity u can be rewritten as a function of h as

$$u = \dot{h} r' / h' \equiv \frac{a_c r_\oplus \sin \alpha_n \cos \alpha_n h}{\sqrt{\mu_\odot^2 - 2 a_c r_\oplus (\cos^2 \alpha_n + 1) h^2}} \quad \text{with } \alpha_n \neq \{-\pi/2, 0, \pi/2\} \text{ rad} \quad (20)$$

whereas, from Eq. (8), the transverse component of the spacecraft velocity is

$$v = \frac{a_c r_\oplus (\cos^2 \alpha_n + 1) h}{\mu_\odot - \sqrt{\mu_\odot^2 - 2 a_c r_\oplus (\cos^2 \alpha_n + 1) h^2}} \quad \text{with } \alpha_n \neq \{-\pi/2, 0, \pi/2\} \text{ rad} \quad (21)$$

Note that the two Eqs. (20) and (21) do not satisfy the initial conditions for a circular parking orbit. This is a consequence of the approximation $\dot{u} = 0$ used in development of the analytical model. The same problem also arises in the calculation of the Sun-spacecraft distance r , see Eq. (12) or Eq. (15), whose initial value is different from that given by Eqs. (11) when $h = h_0$ or $\chi = \chi_0$. Examples of initial errors in terms

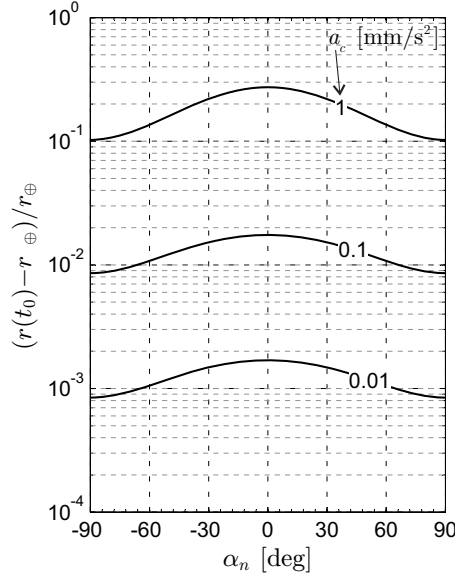


Figure 5: Dimensionless difference between the approximate (see Eq. (12)) and the actual initial Sun-spacecraft distance.

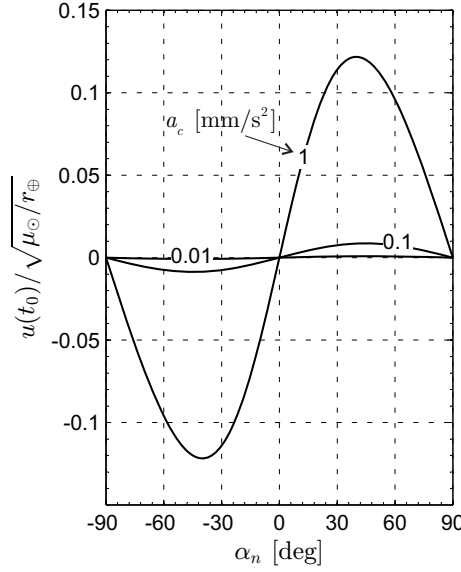


Figure 6: Dimensionless difference between the approximate (see Eq. (20)) and the actual initial E-sail radial component of velocity.

of distance and radial velocities, obtained with Eq. (12) and Eq. (20), are shown in dimensionless form in Figs. 5-6, assuming $a_0 = r_\oplus$. The difference between $r(t_0)$ and a_0 is always less than 2% of r_\oplus as long as $a_c < 0.1 \text{ mm/s}^2$. Moreover, the dimensionless error involving the initial radial distance (or radial velocity) tends to zero when the characteristic acceleration approaches zero, in agreement with Eqs. (12) and (20) in the limit as $a_c \rightarrow 0$ (Keplerian case).

2.2. Validation of Trajectory Approximation

The accuracy of the approximate mathematical model discussed in the previous section is now checked by comparing the results given by the analytical relations, with those deriving from a numerical integration of

the equations of motion. To this end, Eqs. (4)-(7) have been integrated in double precision using a variable order Adams-Bashforth-Moulton solver scheme [26, 27] with absolute and relative errors of 10^{-12} .

The simulation procedure may be summarized as follows. For a given pair $\{\alpha_n, a_c\}$, the equations of motion (4)-(7) (with initial conditions of Eqs. (11), where $a_0 = r_\oplus = 1$ au) are integrated in a time interval $t \in [0, 10]$ years. The corresponding (actual) values of the state variables are indicated with subscript “num”. The function $\chi = \chi(t)$, calculated within the same time interval by combining Eqs. (10) and (14), is substituted into Eqs. (12) and (17) to obtain the time variation of r and θ . The spacecraft position vector is written as

$$\mathbf{r} = r \cos \theta \hat{\mathbf{i}}_x + r \sin \theta \hat{\mathbf{i}}_y \quad (22)$$

where $\hat{\mathbf{i}}_x$ and $\hat{\mathbf{i}}_y$ are the unit vectors of a heliocentric reference frame $\mathcal{T}_c(O; x, y)$ whose x -axis coincides with the Sun-spacecraft line at time t_0 , see Fig. 7. The dimensionless distance d between the exact (numerical)

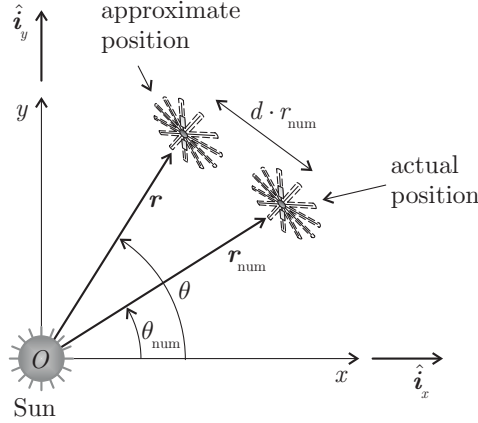


Figure 7: Heliocentric inertial reference frame and relative (dimensionless) distance.

and the approximate (analytical) position, is obtained at each time instant t as

$$d(a_c, \alpha_n, t) = \frac{\sqrt{(r \cos \theta - r_{\text{num}} \cos \theta_{\text{num}})^2 + (r \sin \theta - r_{\text{num}} \sin \theta_{\text{num}})^2}}{r_{\text{num}}} \quad (23)$$

The maximum value of d in the time interval $t \in [0, 10]$ years is

$$d_{\text{max}}(a_c, \alpha_n) \triangleq \max_t \{d(a_c, \alpha_n, t)\} \quad (24)$$

Note that d_{max} is substantially different from the index ρ introduced by [12], since in the latter case the comparison involved the radial distance for a fixed value of angular coordinate θ .

Figure 8 shows the variation of d_{max} with α_n for some (small) values of characteristic acceleration a_c . The maximum dimensionless error is obtained, nearly independent of a_c , when $\alpha_n \approx -45$ deg for an orbit lowering ($\alpha_n < 0$), and $\alpha_n \approx 45$ deg for an orbit raising ($\alpha_n > 0$). Those values of α_n maximize the magnitude of the transverse acceleration a_θ , see Fig. 3(b). In fact, enforcing the necessary condition $\partial a_\theta / \partial \alpha_n = 0$ in Eq. (3), the result is $\alpha_n = \pm 45$ deg.

Figure 8 also confirms that the proposed analytical model approximates reasonably well the actual E-sail dynamics, especially when the characteristic acceleration is sufficiently small. In fact, when $a_c < 0.1$ mm/s², the value of d_{max} is below 10%, that is, the distance between the actual and the approximate E-sail position is less than $r_{\text{num}}/10$. On the other hand, when $a_c < 0.01$ mm/s², the maximum value of the distance error reduces to $d_{\text{max}} < 0.5\%$ only.

The capability of estimating the polar form of the spacecraft trajectory is now checked by first calculating the dimensionless radial error ρ corresponding to a given polar angle θ

$$\rho(a_c, \alpha_n, \theta) = \frac{|r_{\text{num}} - r|}{r_{\text{num}}} \quad (25)$$

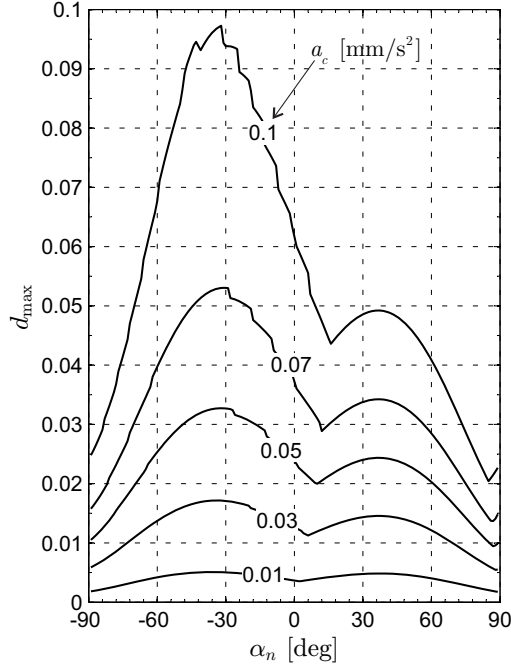


Figure 8: Dimensionless distance error d_{\max} as a function of pitch angle and characteristic acceleration, see Eq. (24).

and then finding its maximum value as a function of the pair $\{a_c, \alpha_n\}$ as

$$\rho_{\max}(a_c, \alpha_n) \triangleq \max_{\theta} \{\rho(a_c, \alpha_n, \theta)\} \quad (26)$$

The variation of ρ_{\max} with $\{a_c, \alpha_n\}$ is shown in Fig. 9 for $a_0 = r_{\oplus}$, assuming (again) a flight time of 10 years. When $a_c = 0.1 \text{ mm/s}^2$, the dimensionless radial error is slightly less than 2% of the actual radial distance r_{num} . An improvement of the accuracy for the proposed analytical model is possible, as is discussed in the next section.

3. Improvement of Trajectory Approximation

Figure 10 shows the actual (solid line) and approximate (dash line) variation of the radial distance r as a function of the angular coordinate θ when $a_c = \{0.01, 0.1\} \text{ mm/s}^2$, assuming $a_0 = r_{\oplus}$, $\alpha_n = 45 \text{ deg}$, and a flight time of 10 years. In particular, the dash line is obtained using Eqs. (15) and (17). Similar results are obtained for all of the pitch angles used in the simulations, provided a_c takes a small value, less than about 0.1 mm/s^2 . The function $r = r(\theta)$ (solid line) is characterized by a secular variation with a superimposed oscillatory behavior, with a period of about $2\pi \text{ rad}$, see Fig. 10. The secular variation is accurately described by the two analytical approximations of Eqs. (15) and (17), which, however, are unable to capture the short-period oscillation. The latter is due to a variation of angular momentum caused by the propulsive acceleration effect, and may be simply and effectively modelled with the aid of an additional term Δr in the form

$$\Delta r \triangleq \mathcal{A} \cos \theta + \mathcal{B} \sin \theta \quad (27)$$

such that, see also Eq. (15), the equation of the Sun-spacecraft distance becomes

$$r = \frac{\mu_{\odot}}{a_c r_{\oplus} (\cos^2 \alpha_n + 1)} \left[1 - \sqrt{1 - \frac{2 a_c r_{\oplus} (\cos^2 \alpha_n + 1) h^2}{\mu_{\odot}^2}} \right] + \mathcal{A} \cos \theta + \mathcal{B} \sin \theta \quad (28)$$

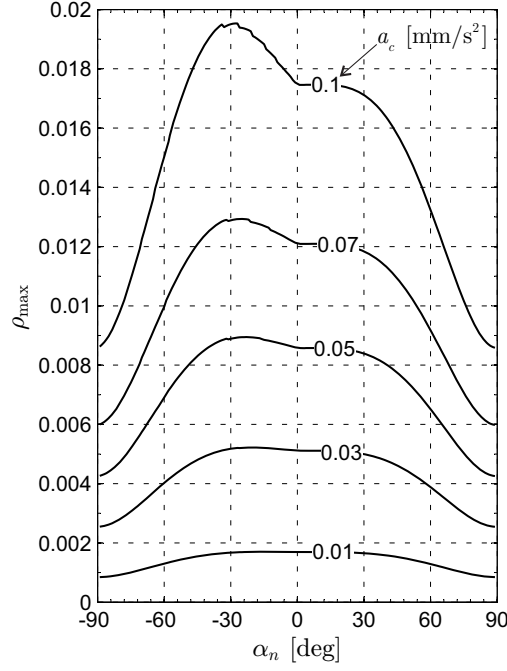


Figure 9: Dimensionless radial distance error ρ_{\max} as a function of the pitch angle and characteristic acceleration, see Eq. (26).

where \mathcal{A} and \mathcal{B} are constant terms to be chosen such that r and \dot{r} meet the initial conditions of Eqs. (11). In particular, note that

$$\dot{r} = \frac{a_c r_{\oplus} \sin \alpha_n \cos \alpha_n h}{\sqrt{\mu_{\odot}^2 - 2 a_c r_{\oplus} (\cos^2 \alpha_n + 1) h^2}} + \frac{4 h a_c^2 r_{\oplus}^2 (\mathcal{B} \cos \theta - \mathcal{A} \sin \theta) (\cos^2 \alpha_n + 1)^2}{\mu_{\odot}^2 \left(1 - \sqrt{1 - \frac{2 a_c r_{\oplus} (\cos^2 \alpha_n + 1) h^2}{\mu_{\odot}^2}} \right)^2} \quad (29)$$

where the first term in the right hand side coincides with the expression of u given by Eq. (20), whereas Eqs. (5) and (12) have been used to obtain the expression of $\dot{\theta} = \dot{\theta}(h)$ in the second term of preceding equation.

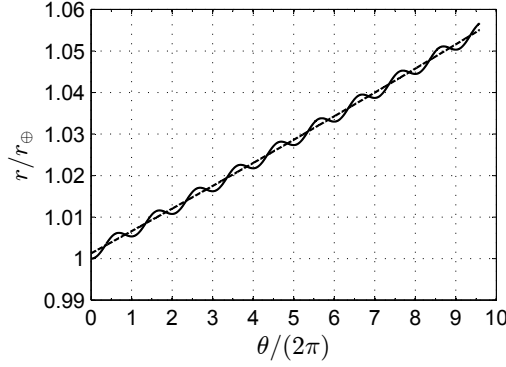
Since $r_0 = a_0$ and $h_0 = \sqrt{\mu_{\odot} a_0}$, from Eq. (28) the value of \mathcal{A} is

$$\mathcal{A} = a_0 \left[1 + \left(\frac{\mu_{\odot}}{a_c r_{\oplus} a_0} \right) \frac{1 - \sqrt{\left(\frac{2 a_c r_{\oplus} a_0}{\mu_{\odot}} \right) (\sin^2 \alpha_n - 2) + 1}}{\sin^2 \alpha_n - 2} \right] \quad (30)$$

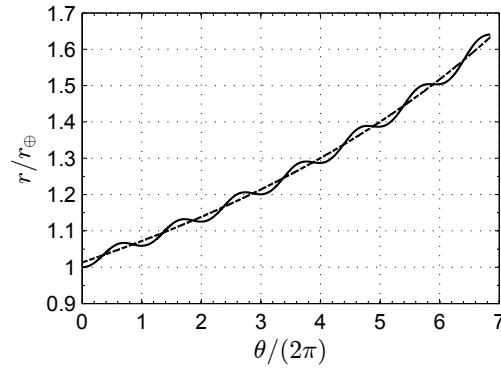
Likewise, recalling that $\dot{r}_0 = 0$, Eq. (29) provides

$$\mathcal{B} = - \frac{\mu_{\odot} \sin \alpha_n \cos \alpha_n \left(\sqrt{1 - \frac{2 a_c r_{\oplus} a_0 (1 + \cos^2 \alpha_n)}{\mu_{\odot}}} - 1 \right)^2}{a_c r_{\oplus} (\cos^2 \alpha_n + 1)^2 \sqrt{1 - \frac{2 a_c r_{\oplus} a_0 (1 + \cos^2 \alpha_n)}{\mu_{\odot}}}} \quad (31)$$

To summarize, the refined parametric version of the propelled trajectory is given by Eqs. (17) and (28), where the two constants \mathcal{A} and \mathcal{B} are obtained from Eqs. (30) and (31), respectively. The new approximation of the radial velocity component u is given by Eq. (29), while the transverse component is $v = h/r^2$, with r obtained from Eq. (28).



(a) $a_c = 0.01 \text{ mm/s}^2$.



(b) $a_c = 0.1 \text{ mm/s}^2$.

Figure 10: Radial distance vs. polar angle when $\alpha_n = 45 \text{ deg}$, $a_0 = r_\oplus$, and a flight time of 10 years. Numerical (solid line) and approximate (dash line) solution.

3.1. Model Validation and Comparison with Literature Results

The refined approximation discussed in the last section is able to considerably reduce the dimensionless radial error ρ_{\max} defined by Eq. (25). This is clearly shown by comparing the results reported in Fig. 9 with those obtained with the refined approach, see Fig. 11, using the same initial conditions for the two cases (i.e. $a_0 = r_\oplus$, and a flight time of 10 years). In particular, Fig. 11 shows that, when $a_c = 0.1 \text{ mm/s}^2$, ρ_{\max} is reduced by about 20% when compared with the previous approximation. The error reduction exceeds 80% when $a_c = 0.03 \text{ mm/s}^2$. The effectiveness of the refined expressions is confirmed by Figs. 12(a)-12(b) that show $r = r(\theta)$ in an orbit raising of 10 years with $a_0 = r_\oplus$, $\alpha_n = 45 \text{ deg}$ and two different characteristic accelerations. In particular, the solid line refers to a numerical simulation, while the dash line is obtained using Eq. (28). For comparative purposes, the same figures also illustrate, with a dash-dot line, the results obtained with the asymptotic expansion method (without rectification) discussed by [23]. Note that, by construction, the latter procedure gives accurate results as long as the characteristic acceleration and the polar angle are sufficiently small. On the other hand, when θ (or a_c) increases, the approximation given by the asymptotic expansion method substantially differs from the (actual) numerical results.

The refined analytic approximation accurately captures the short period oscillation of $r = r(\theta)$, much better than the asymptotic expansion method without rectification. The new results are even nearly coincident with the exact (numerical) solution when $a_c = 0.01 \text{ mm/s}^2$, see Fig. 11. Even though the asymptotic expansion method may substantially reduce the dimensionless error with the introduction of a suitable number of rectifications [23], the significance of the new results is confirmed by the high degree of accuracy obtained with a simple, analytical, relation.

A natural extension of this work involves an analysis of the solar wind (spatial and temporal) variability on the spacecraft trajectory by means of the previous analytical approach. In this context, [28] have proposed

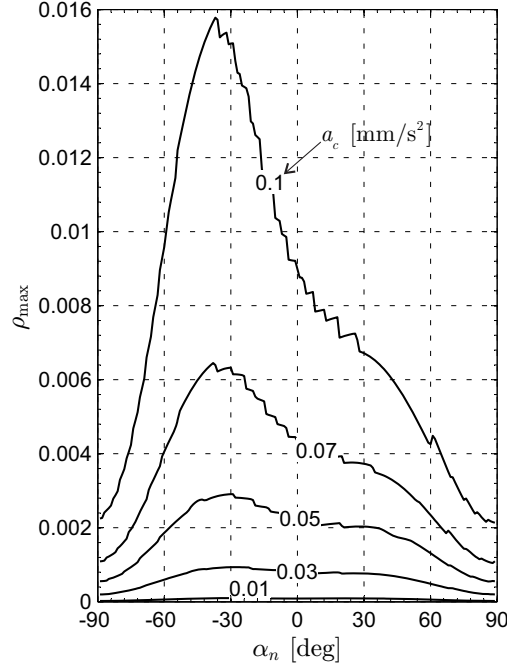


Figure 11: Refined analytical approximation: dimensionless radial distance error ρ_{\max} as a function of α_n and a_c .

an interesting mathematical model for estimating the solar wind characteristics necessary to evaluate the E-sail thrust vector as a function of time, deep-space position and pitch angle.

4. Conclusions

The heliocentric trajectory of an electric solar wind sail with a low propulsive acceleration magnitude may be described by means of analytical relations useful for a preliminary mission design. The assumptions made in the analysis are to consider a circular parking orbit, a two-dimensional motion and an electric solar wind sail with a constant pitch angle. The proposed model is able to capture the short-term variation of the Sun-spacecraft distance induced by the propulsive acceleration. The simulation results have shown that the new model approximates with a high degree of accuracy the actual (simulated) spacecraft trajectory, especially when the spacecraft characteristic acceleration is sufficiently small.

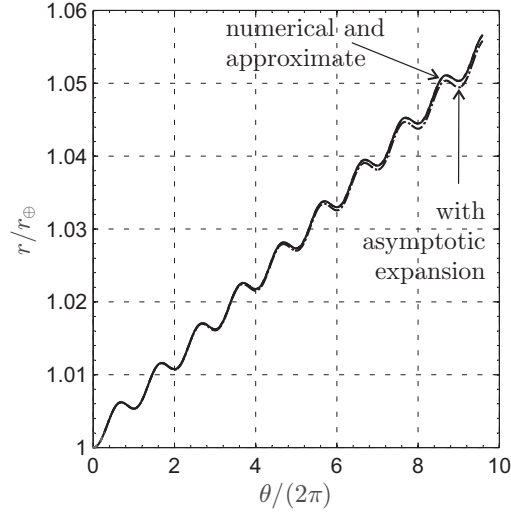
The results illustrated in this paper extend and refine the recent models from the literature, still maintaining a simple (and elegant) form of the final relations. Additional terms could also be added in the future to deal with more complex situations, including the case of a medium-high value of the propulsive acceleration magnitude, that is a characteristic acceleration of about one millimeter per square seconds.

Acknowledgments

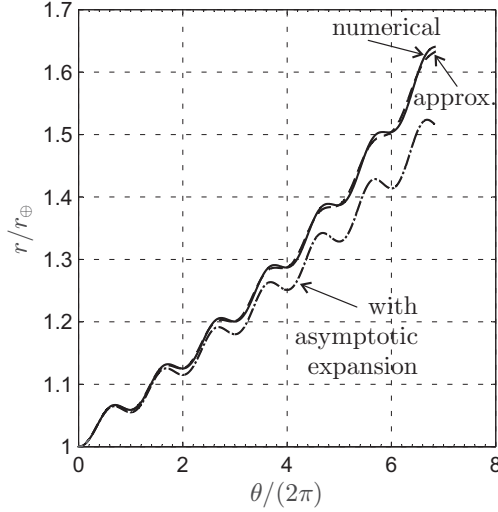
Mingying Huo wishes to thank Shanghai Academy of Spaceflight Technology (NO.SAST2016039), and the Open Fund of National Defense Key Discipline Laboratory of Micro-Spacecraft Technology (Grant Number HIT.KLOF.MST.201607). The authors are indebted to Mr. Lorenzo Niccolai for the results analysis using the asymptotic expansion method.

References

- [1] D. Izzo, Lambert's problem for exponential sinusoids, *Journal of Guidance, Control, and Dynamics* 29 (5) (2006) 1242–1245, doi: 10.2514/1.21796.



(a) $a_c = 0.01 \text{ mm/s}^2$.



(b) $a_c = 0.1 \text{ mm/s}^2$.

Figure 12: Radial distance vs. polar angle when $\alpha_n = 45 \text{ deg}$, $a_0 = r_\oplus$, and a flight time of 10 years. Numerical vs. approximate solution.

- [2] J. Roa, J. Peláez, J. Senent, New analytic solution with continuous thrust: Generalized logarithmic spirals, *Journal of Guidance, Control, and Dynamics* 39 (10) (2016) 2336–2351, doi: 10.2514/1.G000341.
- [3] N. Markopoulos, Analytically exact non-keplerian motion for orbital transfers, in: *Astrodynamics Conference, Guidance, Navigation, and Control*, Scottsdale, AZ, 1994, paper AIAA 94-3758.
- [4] A. E. Petropoulos, J. A. Sims, A review of some exact solutions to the planar equations of motion of a thrusting spacecraft, in: *2nd International Symposium on Low-Thrust Trajectory (LoTus-2)*, Toulouse, France, 2002.
- [5] C. R. McInnes, Orbits in a generalized two-body problem, *Journal of Guidance, Control, and Dynamics* 26 (5) (2003) 743–749, doi: 10.2514/2.5129.
- [6] A. E. Petropoulos, J. M. Longuski, Shape-based algorithm for the automated design of low-thrust, gravity assist trajectories, *Journal of Spacecraft and Rockets* 41 (5) (2004) 787–796, doi: 10.2514/1.13095.
- [7] B. Wall, B. Conway, Shape-based approach to low-thrust rendezvous trajectory design, *Journal of Guidance, Control, and Dynamics* 32 (1) (2009) 95–102, doi: 10.2514/1.36848.
- [8] D. Novak, M. Vasile, Improved shaping approach to the preliminary design of low-thrust trajectories, *Journal of Guidance, Control, and Dynamics* 34 (1) (2011) 128–147, doi: 10.2514/1.50434.
- [9] E. E. Wiesel, S. Alfano, Optimal many-revolution orbit transfer, *Journal of Guidance, Control, and Dynamics* 8 (1) (1985) 155–157, doi: 10.2514/3.19952.
- [10] S. Alfano, J. D. Thorne, Circle-to-circle constant-thrust orbit raising, *Journal of the Astronautical Sciences* 42 (1) (1994)

- [11] R. H. Battin, An Introduction to the Mathematics and Methods of Astrodynamics, revised edition Edition, Education Series, AIAA, New York, 1999, p. 418, ISBN: 978-1-56347-342-5.
- [12] A. A. Quarta, G. Mengali, Trajectory approximation for low-performance electric sail with constant thrust angle, *Journal of Guidance, Control, and Dynamics* 36 (3) (2013) 884–887, doi: 10.2514/1.59076.
- [13] P. Janhunen, Electric sail for spacecraft propulsion, *Journal of Propulsion and Power* 20 (4) (2004) 763–764, doi: 10.2514/1.8580.
- [14] P. Janhunen, et al., Electric solar wind sail: Towards test missions, *Review of Scientific Instruments* 81 (11) (2010) 111301 (1–11), doi: 10.1063/1.3514548.
- [15] K. Yamaguchi, H. Yamakawa, Study on orbital maneuvers for electric sail with on-off thrust control, *Aerospace Technology Japan* 12 (2013) 79–88, doi: 10.2322/astj.12.79.
- [16] M. Huo, G. Mengali, A. A. Quarta, Electric sail thrust model from a geometrical perspective, *Journal of Guidance, Control and Dynamics* 41 (3) (2018) 735–741, doi: 10.2514/1.G003169.
- [17] K. Yamaguchi, H. Yamakawa, Electric solar wind sail kinetic energy impactor for near earth asteroid deflection mission, *The Journal of the Astronautical Sciences* 63 (1) (2016) 1–22, doi: 10.1007/s40295-015-0081-x.
- [18] A. A. Quarta, G. Mengali, Minimum-time trajectories of electric sail with advanced thrust model, *Aerospace Science and Technology* 55 (2016) 419–430, doi: 10.1016/j.ast.2016.06.020.
- [19] P. Toivanen, P. Janhunen, Thrust vectoring of an electric solar wind sail with a realistic sail shape, *Acta Astronautica* 131 (2017) 145–151, doi: 10.1016/j.actaastro.2016.11.027.
- [20] P. Janhunen, A. A. Quarta, G. Mengali, Electric solar wind sail mass budget model, *Geoscientific Instrumentation, Methods and Data Systems* 2 (1) (2013) 85–95, doi: 10.5194/gi-2-85-2013.
- [21] G. Mengali, A. A. Quarta, G. Alias, A graphical approach to electric sail mission design with radial thrust, *Acta Astronautica* 82 (2) (2013) 197–208, doi: 10.1016/j.actaastro.2012.03.022.
- [22] A. A. Quarta, G. Mengali, Analysis of electric sail heliocentric motion under radial thrust, *Journal of Guidance, Control and Dynamics* 39 (6) (2016) 1431–1435, doi: 10.2514/1.G001632.
- [23] L. Niccolai, A. A. Quarta, G. Mengali, Two-dimensional heliocentric dynamics approximation of an electric sail with fixed attitude, *Aerospace Science and Technology* 71 (2017) 441–446, doi: 10.1016/j.ast.2017.09.045.
- [24] C. Bombardelli, G. Baú, J. Peláez, Asymptotic solution for the two-body problem with constant tangential thrust acceleration, *Celestial Mechanics and Dynamical Astronomy* 110 (3) (2011) 239–256, doi: 10.1007/s10569-011-9353-3.
- [25] L. Niccolai, A. A. Quarta, G. Mengali, Solar sail trajectory analysis with asymptotic expansion method, *Aerospace Science and Technology* 68 (2017) 431–440, doi: 10.1016/j.ast.2017.05.038.
- [26] L. F. Shampine, M. K. Gordon, *Computer Solution of Ordinary Differential Equations: The Initial Value Problem*, W. H. Freeman, San Francisco, 1975, Ch. 10.
- [27] L. F. Shampine, M. W. Reichelt, The matlab ode suite, *SIAM Journal on Scientific Computing* 18 (1) (1997) 1–22 .
- [28] P. K. Toivanen, P. Janhunen, Electric sailing under observed solar wind conditions, *Astrophysics and Space Sciences Transactions* 5 (1) (2009) 61–69, doi: 10.5194/astra-5-61-2009.